Experimental, DFT dimeric modeling and AIM study of H-bond-mediated composite vibrational structure of Chelidonic acid

Shivanand S. Malaganvi, Jayashree Tonannavar (Yenagi), J. Tonannavar *

Vibrational Spectroscopy Group, Department of Physics, Karnatak University, Dharwad, 580 003, India

ABSTRACT

The composite vibrational structure near 3650–3200 and 3000–2400 cm^{-1} in the observed IR absorption spectrum of Chelidonic acid has been explained in terms of *intra*- and *inter*-molecular $-O-H \cdots O$ H-bonding attributed to monomer and dimer species computed at B3LYP/6–311++G(d,p) level. Three of the six dimer species derived out of ten monomeric components have shown both *intra*- and *inter*-molecular H-bonding. Vibrational modes of the monomer and dimer species are satisfactorily identified with the observed IR and Raman bands including frequency shifts associated with the H-bondings. The H-bond interactions in the monomer and dimer species have been characterized in terms of electron density, $\rho(\mathbf{r})$, its Laplacian, $\nabla^2\rho(\mathbf{r})$ and potential energy density at the $O \cdots H$ bond critical points (BCPs) based on the Atoms in Molecules (AIM) theory. The attractive (van der Waals, H-bonds) and repulsive steric clash (SC) interactions are explained using computed reduced density gradient values from the noncovalent interaction (NCI) method. The AIM analysis confirms the presence of the *intra*- and *inter*-molecular H-bondings in the monomer/dimer species. The natural bond orbital (NBO) analysis of the natural charges and stabilization energy of the H-bonds for the dimer species further points to the stronger *inter*- than *intra*-molecular H-bonding.

1. Introduction

The *intra*- and *inter*-molecular H-bonding in carboxylic acid (CBA) dimeric units are of unwavering interest and are commonly characterized by IR spectroscopic studies of $-O-H$ stretching vibrations in the region 4000–400 cm^{-1} [1-6]. The most common form of H-bonding is the dimerization between the two carboxylic groups often cyclically bound by a local center of inversion, resulting in a larger down-shift of the $-O-H$ stretching frequency of the dimeric carboxylic acids (3000–2500 cm^{-1}) [1]. Diverse complexes such as these dimeric species governed by the structure and strength of the H-bonds have been largely the subject of intense experimental and theoretical studies with wider implications in multidisciplinary subjects [7, 8, 9, 10, 11]. In addition to their biological interest and anti-carcinogenic drug properties, the study of homo-/hetero-complexes of CBAs in gaseous, liquid, and solid states have provided insights into the nature of noncovalent interactions including $-O-H \cdots O=C$ interactions [12, 13, 14, 15]. In the recent past, studies on simple CBA systems, for example, the formic acid dimer species participating in strong to weak *inter*-molecular interactions have been reported [1, 2, 3, 4, 5, 6, 7, 8, 9, 10, 11, 12, 13, 14, 15]. However, there have been apparently fewer similar investigations of the H-bond induced

composite vibrational structure of the benzenedicarboxylic acids (BDAs) [16, 17, 18, 19, 20, 21]. Recently, Karabacak *et al* have assigned IR and Raman modes of the solid Isophthalic acid on the basis of computed monomers and $O-H \cdots O$ bound dimer species [19]. *Ab initio* predictions of the effects of temperature and solvation on the dimerization of benzoic acid have been reported by Taylor *et al* [22]. They conclude that benzoic acids form strong H-bonds with each other in different complexes but a cyclic dimer among them is the most stable configuration. Martsinovich *et al* have reported modeling of the self-assembly of BDAs using Monte-Carlo and molecular dynamics simulations (MD) [23]. The structural studies by R. Alcala *et al*, J.L. Derissen and by M. He *et al* on Isophthalic acid and 5-Fluoroisophthalic acid also support the ordered cyclic structures stabilized by double $O-H \cdots O$ bonds between two carboxylic groups [24, 25, 26].

In the present work, we report extensive study of the structural, vibrational and electronic properties of the conformational and dimerization aspects of H-bonded species of Chelidonic acid (CA for short; it is also called 4-Oxo-4H-pyran-2,6-dicarboxylic acid, $C_7H_4O_6$, see Fig. 1). The CA is a pyran skeleton with dicarboxylic acid group and is a suitable intermediate in certain synthesis work but more importantly its pharmacological effects and therapeutic potential have been demonstrated
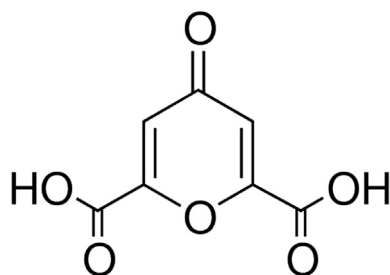
Fig. 1. Molecular structure of Chelidonic acid.

[27, 28, 29]. From structural and spectroscopic view-points, the CA is an attractive candidate for the investigation of H-bonding in the formation of dimer species. This has been borne out by the observation of broad IR absorption bands near 3650–3200 cm^{-1} with a series of bands in 3000–2400 cm^{-1} (Fig. 2(a), see also Fig. S1, Supplementary Material). This vibrational structure extending from 3650 to 2400 cm^{-1} including two IR and Raman bands near 1648 and 1723 cm^{-1} is the apparent manifestation of *intra-* in monomer and both *intra-* and *inter*-molecular O−H···O bonding in the dimer species of CA (see Fig. 2). We have computed all the possible dimer species at B3LYP and BP86 methods combined with the 6-31G(d) and 6–311++G(d,p) basis sets, yielding six dimer species of which three are *inter*-molecularly H-bonded and three are mixed *inter-* and *intra*-molecularly H-bonded species. In the proposed dimer models, the two carboxylic motifs simultaneously act as H-bond donor and acceptor. The *inter*-H-bonds are strong since computed interaction energy per bond is 9 kcal/mol. As a consequence, the −O−H and −C=O stretching modes have shown large red-shifts in frequencies with broadening of the bands. We have shown that the simulated IR bands spectra derived from six dimer species of CA are in agreement with the measured spectrum in the 3700–400 cm^{-1}. Furthermore, we have characterized the *inter-* and *intra*-H-bonding in the dimer species as noncovalent interactions by the electron density topological analysis by employing the quantum theory of Atoms in Molecules (AIM) and non-covalent interaction (NCI) methods. The charge transfer in the monomer and dimer species due to the H-bonding interactions is explained using the natural bond orbital (NBO) analysis.

2. Methods

2.1. Experimental methods

The sample of Chelidonic acid (Sigma-Aldrich, part of Merck; assay, 98.0%; mp 265 °C) was used as received. The IR absorption spectrum of the sample was measured at room temperature using standard KBr pellet technique. The spectrum was measured at 2 cm^{-1} resolution with 100 scans in the range 4000–400 cm^{-1} on a Thermo-Fisher *Nicolet* 6700 FT-IR spectrometer equipped with a KBr beam splitter, a ETC EverGlo mid-IR radiation source, and a deuterated L-alanine doped triglycine sulfate (DLaTGS) detector. The Raman spectrum was measured from 3500 – 100 cm^{-1} at a spectral resolution of 2 cm^{-1} with a Thermo-Fisher *NXR* 6700 FT-Raman module spectrometer, equipped with a diode-pumped air cooled Nd:YVO$_4$ laser source (1064 nm excitation line) and a LN$_2$ cooled high-performance Ge detector. The spectra were averaged over 500 scans. Both the spectrometers were purged with nitrogen to remove the interference due to the atmospheric CO$_2$ and moisture. The solid-phase near-IR (NIR) spectrum of Chelidonic acid was measured in the 4000–8000 cm^{-1} region and for the sake of brevity, the analysis has been presented in the section S10 (see also Fig. S10a).

2.2. Computational methods

All the electronic structure calculations were performed using the *Gaussian 09W, GaussView 5, Multiwfn, VMD* and *Chemcraft* suite of

programs [30, 31, 32, 33, 34, 35]. Molecular structure of CA is presented in Fig. 1. Initially, the conformational search was performed by a relaxed potential energy surface scan (PES) at B3LYP/6-31G(d) level by rotating the two −COOH groups from 0° to 350° with step of 10° (see Fig. S11). The initial PES scan at B3LYP/6-31G(d) level reduced the computational cost. However, this level for H-bonded structures is known to produce less accurate geometrical and energetic parameters when compared to the experimental values. Moreover, in addition to the inclusion of the electron correlation effects on geometry optimization as defined in the B3LYP method, the use of flexible basis set with polarization and diffuse functions on hydrogen atom orbitals is necessary for the accurate description of H-bond interactions. These basis set requirements are usually met by using the flexible and extended basis set 6–311++G(d,p). Therefore, in the present study, we used 6–311++G(d,p) basis set for the calculations. We found ten minima on the PES which were again optimized at the B3LYP/6–311++G(d,p) level. Moreover, the harmonic frequency analysis at the same level confirmed all the ten minima as true stationary points, yielding a total of ten monomers (Fig. 3). The observed nature and intensity of the IR and Raman stretching modes of −O−H and −C=O groups near 3650–2400 cm^{-1} and 1800–1600 cm^{-1} region strongly suggest that the modes would arise in H-bonded dimer species from the monomers. As a next logical step, we constructed a total of six dimer species, D_i (i = 1 to 6) that are shown in Fig. 4. The dimer species D_1, D_2 and D_3 are *inter*-molecularly bonded via −O−H···O=C and D_4, D_5 and D_6 are both *intra-* and *inter*-molecularly bonded, with the *intra*-molecular H-bond referring to −O−H···O(pyran ring). The optimized geometries of the most stable monomer and dimer species of CA with the numbering scheme are presented in Fig. 5. Calculations at BP86/6-31G(d) level were also performed, yielding slightly better frequency values than B3LYP/6–311++G(d,p) values. However, for the reasons already stated above and the B3LYP/6–311++G(d,p) level is known to predict fairly accurate results for AIM analysis, all the results obtained from this level alone will be discussed, though occasionally reference is made to BP86/6-31G(d) results. We computed the strength of the H-bonds as the energy difference between dimer and monomer components (ΔE^{int}, this energy is a measure of strength of the H-bond) and these resultant energies are corrected for the basis-set-superposition-error (BSSE) using the counterpoise (CP) method of Boys and Bernardi [36]. The H-bond interactions in the dimer species have been characterized in terms of electron density, $\rho(\mathbf{r})$, its Laplacian $\nabla^2\rho(\mathbf{r})$ and potential energy density at bond critical points (BCP) using the *Multiwfn* program based on the quantum theory of Atoms in Molecules (AIM) [32, 33] and reduced density gradient, $s(\mathbf{r})$, by the non-covalent interaction (NCI) methods using the *Multiwfn* and *VMD* programs [37, 38, 39, 40, 41, 42, 43, 44, 45, 46, 47, 48]. The nature of electronic charge delocalization accompanied by H-bond formation has been investigated by employing NBO analysis at the B3LYP/6–311++G(d,p) level [49].

3. Results and discussion

3.1. Vibrational and H-bonding analysis

The carboxylic acids show extensive *inter*-molecular H-bonding in the formation of dimer species and as a result, the IR frequency of the −O−H stretching mode shifts toward lower frequency region [1, 2, 3, 4, 5, 6, 7, 8, 9, 10, 11, 12, 13, 14, 15]. Flett and others reported that, whereas the −O−H stretching frequency of monomer species lies near 3600 cm^{-1}, it gives rise to a broad absorption with many sub-bands near 2500–3000 cm^{-1} due to dimeric species [50]. These assignments have been used as reference for the assignments of −O−H stretching mode and other modes of CA. The IR and Raman bands of CA are shown in Fig. 2 (see also Fig. S1, Supplementary Material). To satisfactorily account for the vibrational structure of CA apparently induced by *intra-* and *inter*-molecular H-bonding, we assume dimerization of its monomer components. Accordingly, as a first step, we computed ten possible monomer species
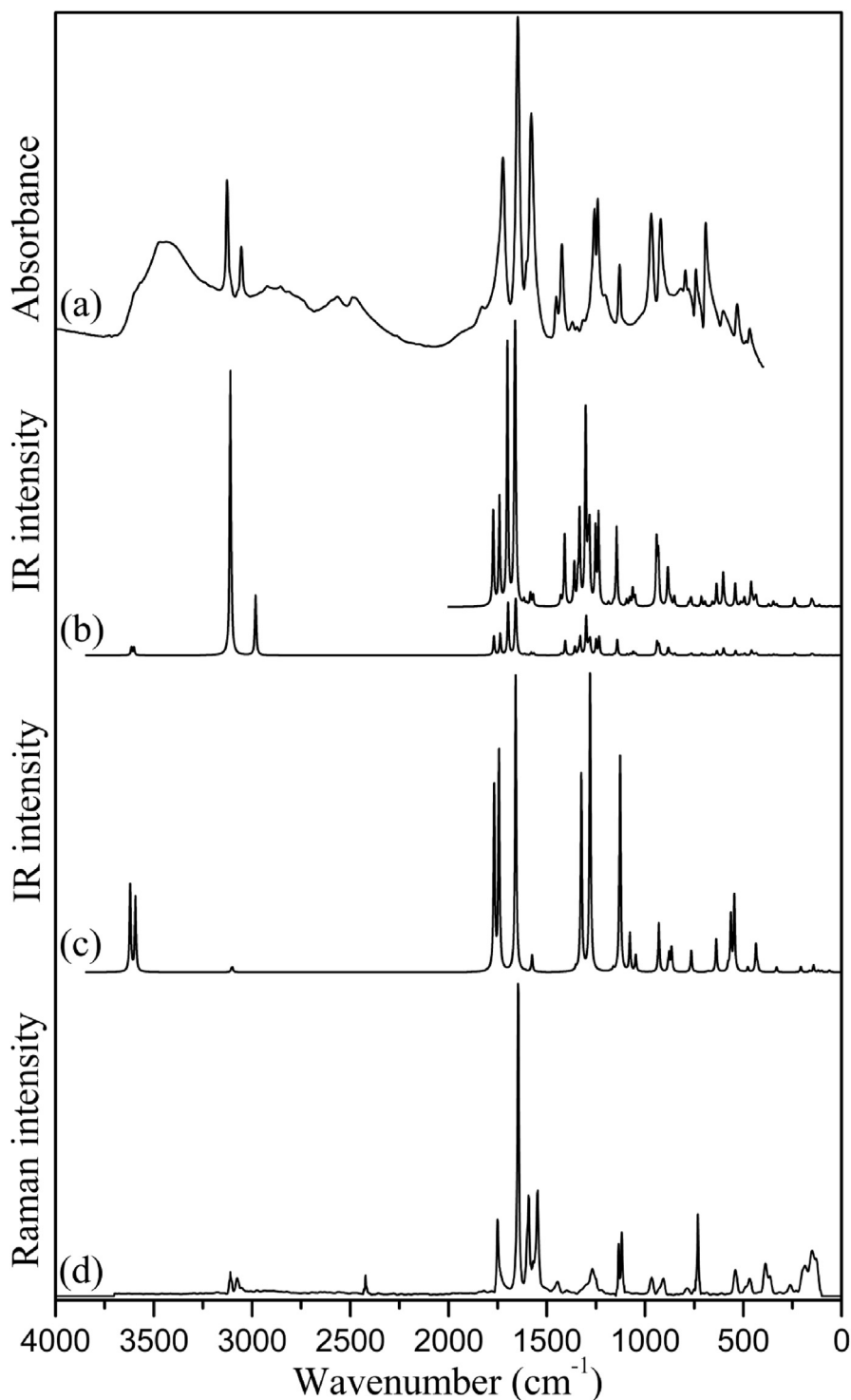
Fig. 2. Experimental FT-IR (a) and simulated IR spectra for D_4 dimer (b) and M_4 monomer (c) species of Chelidonic acid. Experimental FT-Raman spectrum (d) is also shown.

(i.e. conformers), yielding, say, $M_1, M_2,…, M_{10}$, that are shown in Fig. 3. The M_1, M_3, M_8 and M_{10} species belong to C_{2v} symmetry; M_2, M_4, M_5 and M_6 belong to C_s symmetry; M_7 and M_9 belong to C_1 symmetry. The M_1, M_2, M_3 do not show *intra*-molecular H-bonding, whereas, M_4 shows it (see Fig. S2). Except for the Boltzmann populations of M_1, M_2, M_3 and M_4, the populations of other monomer species are too small to be useful for discussion. Therefore, in the second step we computed ten dimer species all only from M_1, M_2, M_3 and M_4 species. Fig. 4 presents D_1, D_2, D_3, D_4, D_5 and D_6 dimer structures; the remaining four dimer species called D_7, D_8,

D_9 and D_{10} are identical and are separately presented in Fig. S3. The analysis of all the dimer species indicated that the computed geometrical, vibrational, AIM, NCI and NBO properties of the $D_7–D_{10}$ dimers are identical to those for the $D_1–D_6$ species. That is to say, $D_7–D_{10}$, dimers are not distinct and they map identically to the $D_1–D_6$ species. Therefore, only $D_1–D_6$ dimer species were chosen for the discussion. The M_4, M_5, M_8 and M_9 have twisted −COOH structure and exhibit *intra*-molecular −O−H···O−C bonding with the oxygen from the pyran ring (see Fig. S2). The M_1 is found to be the most stable and energies of other
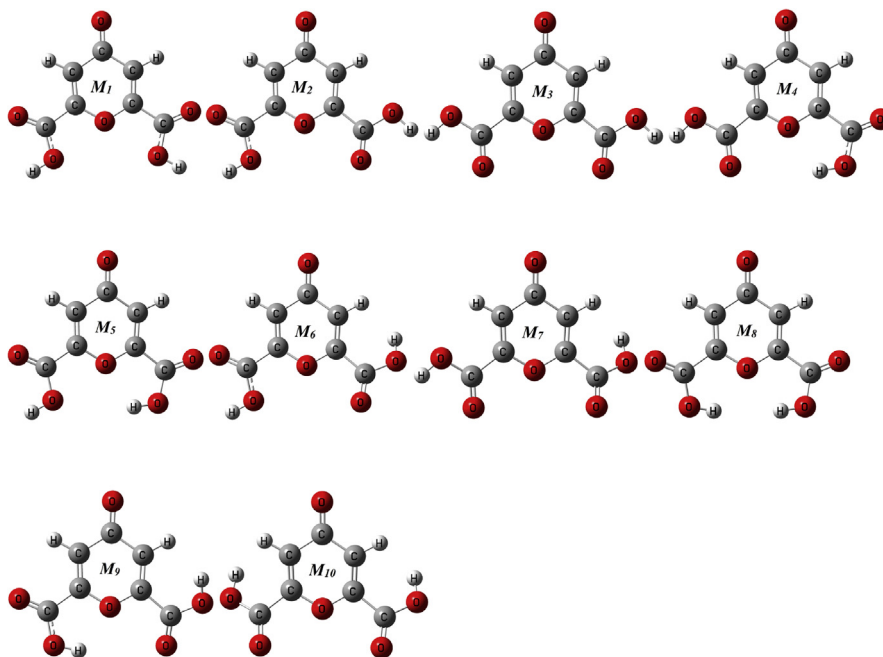
Fig. 3. Optimized structures of ten monomers of Chelidonic acid.
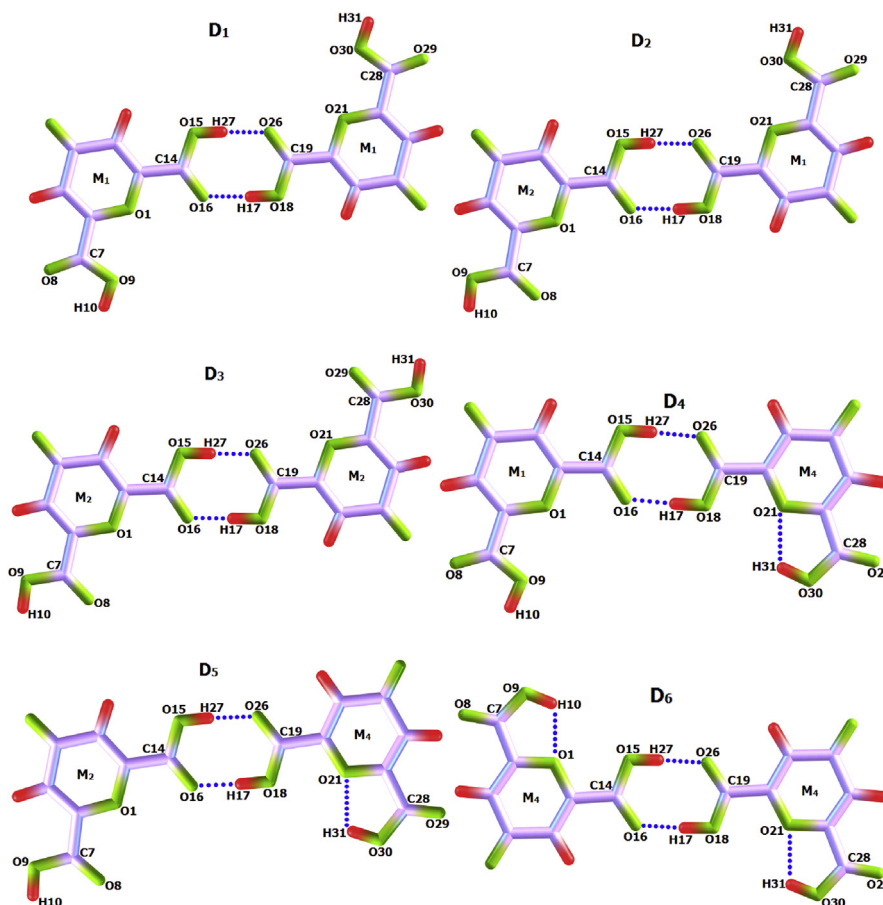
Fig. 4. Optimized structures of six dimer species of Chelidonic acid. *Inter*-H-bonding is in D_1, D_2, D_3; both *intra*- and *inter*-bonding is in D_4, D_5 and D_6.

monomers relative to M_1's are shown in Table 1. The dimer energetics is collected in Table 2. The geometrical parameters of M_1, M_4 and D_4 species are presented in Table 3. All the dimer species exhibit proton transfer

reaction at the *inter*-molecular bonding site. Of the six dimer species, predicted IR bands of D_4, D_5 and D_6 are identified with the observed −O−H stretching bands because they have shown both *intra*- and

Fig. 5. Optimized structures of most stable monomer (a), and dimer (b) of Chelidonic acid.

Table 1
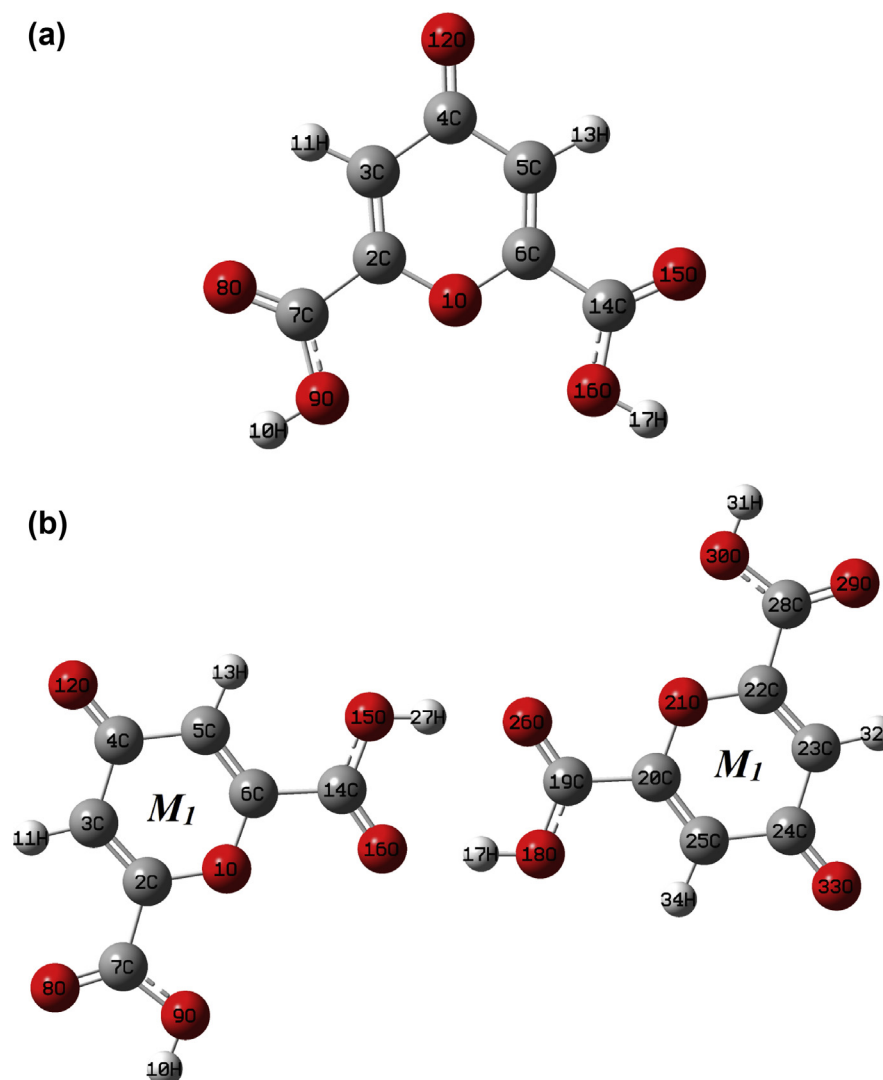Computed Gibbs free energies and relative energies for the ten monomers of Chelidonic acid. The energies are calculated at B3LYP/6–311++G(d,p) level.

Monomers	Gibbs free energy, ΔG (hartree)	Gibbs free energy, ΔG (kcal/mol)	Relative Gibbs free energy, ΔG (kcal/mol)
M_1	-720.638165	-452207.29460007	0.00
M_2	-720.637978	-452207.17725579	-0.12
M_3	-720.637411	-452206.82145791	-0.47
M_4	-720.636174	-452206.04522865	-1.25
M_5	-720.635501	-452205.62291476	-1.67
M_6	-720.627271	-452200.45851158	-6.84
M_7	-720.626495	-452199.97156420	-7.32
M_8	-720.625840	-452199.56054548	-7.73
M_9	-720.625313	-452199.22984797	-8.07
M_{10}	-720.615112	-452192.82862356	-14.47

inter-bonding. For the sake of brevity, only calculated and observed frequencies of the main bands of −O−H and −C=O groups are presented in Table 4 (see also Table S4) [51, 52].

The geometrical criterion for the formation of an −O−H···O bond is the O···H contact distance required to be less than the sum of van der Waals (vdW) radii of O and H, namely, 2.720 Å [53]. In Fig. 4, each dimer species has a double *inter*-bonded O···O bonds involving two −COOH

groups. In all the dimer species, the two O−H···O bond angles are 177° (Table S5). Additionally, the D_4 and D_5 are stabilized by a single *intra*-bond and D_6 is stabilized by two *intra*-bonds. The D_1 is the most stable with the $\Delta E^{int} = $ -17.77 kcal/mol (Table 2). The two O···H and O···O contact distances are calculated at 1.674, 1.672 and 2.672, 2.670 Å respectively (Table S5). The D_2 has $\Delta E^{int} = $ -17.95 kcal/mol. In this dimer the two O15···O26 and O16···O18 bond lengths are nearly close, 2.670 and 2.669 Å. The O26···H27 and O16···H17 distances are calculated at 1.673 and 1.671 Å respectively. The D_3 with $\Delta E^{int} = $ -18.10 kcal/mol is stabilized by two H-bonds with O···H distance at 1.673 Å and the two O···O distances being equal (2.671 Å). In D_4 ($\Delta E^{int} = $ -17.63 kcal/mol) and D_5 ($\Delta E^{int} = $ -17.90 kcal/mol), the O30−H31 group interacts with the pyran ring's oxygen atom, O21, for which the contact distances, O21···H31, are calculated at 2.051 and 2.053 Å respectively (these are not shown in Table S5). The *inter*-molecular O···H and O···O distances are computed at 1.687, 1.654 and 2.682, 2.655 Å for the dimer D_4 and 1.688, 1.654 and 2.683, 2.655 Å for the dimer D_5. With $\Delta E^{int} = $ -17.22 kcal/mol, the D_6 species, in addition to two *inter*-molecular O26···H27 and O16···H17 distances with 1.671 Å, has shown two *intra*-molecular bonds with O1···H10 and O21···H31 at 2.055 Å (these are not shown in Table S5) and the two *inter*-molecular O···O distances are computed at 2.669 and 2.670 Å. It may be noted that, although the relative energies of the six dimer species are not negligible, the differences in the ΔE^{int} are rather very small and this may be attributed to the

Table 2
Computed Gibbs free energies, relative energies and interaction energies for the six dimers of Chelidonic acid. The energies are calculated at B3LYP/6–311++G(d,p) level. The interaction energy (ΔE^{int}) is obtained as the difference between the energy of the complex (i.e. a dimer) and that of the monomer components. The ΔE^{int} values are corrected for basis set superposition error (BSSE).

Dimer	Monomer combinations	Gibbs free energy, ΔG (hartree)	Gibbs free energy, ΔG (kcal/mol)	Relative Gibbs free energy, ΔG (kcal/mol)	Interaction Energy, ΔE^{int} (kcal/mol)
D_1	M_1 with M_1	-1441.281299	-904417.70729484	0.00	-17.77
D_2	M_1 with M_2	-1441.280977	-904417.50523678	-0.20	-17.95
D_3	M_2 with M_2	-1441.280708	-904417.33643673	-0.37	-18.10
D_4	M_1 with M_4	-1441.278555	-904415.98540877	-1.72	-17.63
D_5	M_2 with M_4	-1441.278286	-904415.81660872	-1.89	-17.90
D_6	M_4 with M_4	-1441.275438	-904414.02946166	-3.68	-17.22

differences in the energies of the monomer components and geometries of the −COOH groups involved in the H-bonding. The ΔE^{int} values are

Table 3
Computed geometrical parameters for monomer M_1, M_4 and dimer D_4 of Chelidonic acid. The geometrical parameters are calculated at B3LYP/6–311++G(d,p) level. For comparison of the geometrical parameters in the bonded and non-bonded case, monomers M_1 (free), M_4 (intra-molecularly bonded) and the dimer D_4 (both intra-and inter-molecularly bonded) species were chosen, [a]Ref [56].

Parameter	Monomer		Dimer	[a] Experimental
	M_1	M_4	D_4	Meconic acid
Bond lengths (Å)				
C4−C3	1.468	1.468	1.467	1.431
C4−C5	1.468	1.473	1.470	1.463
C4 = O12	1.223	1.221	1.222	1.245
C3 = C2	1.347	1.345	1.348	1.345
C3−H11	1.082	1.081	1.082	−
C2−O1	1.357	1.363	1.356	1.349
C2−C7	1.497	1.507	1.499	1.501
O1−C6	1.357	1.360	1.355	1.362
C6 = C5	1.347	1.345	1.348	1.363
C6−C14	1.497	1.495	1.496	1.475
C5−H13	1.082	1.081	1.081	−
C7 = O8	1.204	1.199	1.204	1.219
C7−O9	1.343	1.343	1.342	1.309
O9−H10	0.970	0.970	0.970	−
C14 = O15	1.204	1.203	1.317	1.235
C14−O16	1.343	1.345	1.221	1.302
O16−H17	0.970	0.969	−	−
O15−H27	−	−	0.997	−
O26···H27	−	−	1.687	−
O16···H17	−	−	1.654	−
Bond angles (°)				
C3−C4−C5	113.1	113.4	113.1	114.7
C3−C4 = O12	123.5	123.7	123.7	124.1
C5−C4 = O12	123.5	122.9	123.2	121.2
C4−C3 = C2	120.9	120.7	120.8	120.8
C4−C3−H11	119.7	120.0	119.8	−
C2 = C3−H11	119.4	119.3	119.3	−
C3 = C2−O1	123.5	123.2	123.6	123.8
C3 = C2−C7	122.1	124.3	122.0	124.4
O1−C2−C7	114.4	112.5	114.4	111.8
C2−O1−C6	118.2	119.0	118.3	118.0
O1−C6 = C5	123.5	122.7	123.5	122.9
O1−C6−C14	114.4	110.7	111.7	114.9
C5 = C6−C14	122.1	126.6	124.9	122.1
C4−C5 = C6	120.9	121.1	120.9	119.7
C4−C5−H13	119.7	118.9	119.2	−
C6 = C5−H13	119.4	120.0	120.0	−
C2−C7 = O8	122.8	121.7	122.7	111.9
C2−C7−O9	112.7	115.6	112.7	122.0
O8 = C7−O9	124.5	122.7	124.6	126.1
C7−O9−H10	107.3	111.0	107.4	−
C6−C14 = O15	122.8	123.8	112.9	119.2
C6−C14−O16	112.7	111.6	121.8	116.0
O15 = C14−O16	124.5	124.7	125.3	124.8
C14−O16−H17	107.3	107.8	−	−
C14−O15−H27	−	−	110.2	−
O15−H27···O26	−	−	176.7	−
O16···H17−O18	−	−	177.5	−

comparable with the experimental values of the dimerization energy of Benzoic acid, -16.20 kcal/mol, derived from the measurements of its monomer and dimer IR spectra [54, 55]. Table 3 shows the geometrical parameters of M_1, M_4 and D_4 species around the two −COOH groups (see also Fig. 5 and Fig. S6). To the best of our knowledge, there appears to be no crystal structure data for CA in the literature; therefore, it is not untenable to compare the main geometrical parameters of the two −COOH groups in the monomer and dimer species (see Table 3 and Table S5) with the crystal structure data of Isophthalic acid, 5-Fluoroisophthalic acid and Meconic acid [24, 25, 26, 56]. From Table S5, one can see that the bond lengths and angles of the two −COOH groups have shown attendant changes due to the H-bonding.

As shown in Fig. S1 (Supplementary Material), the absorptions in the 3650–2400 cm^{-1} are characterized by a broad band structure with a series of closely-lying bands at 3629, 3601, 3557, 3468, 3418 cm^{-1} and 2962, 2922, 2854, 2814, 2756, 2736 cm^{-1} and 2597, 2564, 2489, 2474 cm^{-1}. We tentatively assign the bands near 3630–3550 cm^{-1} to a free −O−H stretching mode. The bands near 3470–3410 cm^{-1} are assigned to both medium strong inter- and intra-molecularly bound −O−H stretching modes and those near 2970–2470 cm^{-1} to strong inter-molecularly bound −O−H stretching modes. Two strong to medium bands at 3127 and 3055 cm^{-1} are readily assigned to −C−H stretching modes. Further, the strong bands near 1800–1600 cm^{-1} in the IR and Raman spectra being characteristic bands of −C=O stretching modes of −COOH groups are rather broad and red-shifted, indicating the participation of −C=O groups in H-bonding. This is consistent with the assignments for formic acids and benzenedicarboxylic acids that show similar modified vibrational structure upon H-bonding [16, 19, 50]. Computed harmonic frequencies of some of the main bands of M_1, M_4, D_1, D_2, D_3, D_4, D_5 and D_6 species in comparison with the experimental values are presented in Table 4. The computed IR spectra of all the dimer species are shown in Figs. 6a and 6b. It is apparent from Fig. 4 that the H-bond forms a local cyclic −O−H···O=C configuration influencing the −O−H and −C=O stretching modes of the −COOH group with their frequencies showing red-shifts and intensity enhancements (Figs. 6a and 6b). The observed IR bands at 3629 and 3601 cm^{-1} are assigned to the free −O−H stretching vibrations. The corresponding predicted frequencies for the M_1 are 3615 and 3614 cm^{-1}. In going from the monomers to dimers, except for the D_4, D_5 and D_6, these two frequencies show no substantial shift. In D_4, D_5 and D_6, the O30−H31 group is intra-molecularly bonded to the pyran ring oxygen atom O21. This caused a small red-shift in the −O−H stretching frequency predicted at 3601 cm^{-1} for D_4 and D_5 and is tentatively correlated to a broad absorption at 3468 cm^{-1}, the difference in deviation being ∼4%. It is also possible that in the solid phase of CA, the monomeric structures stabilized by intra-molecular H-bonding are not favored and therefore, in the absence of strong experimental evidence, we tentatively assign the bands observed near 3400 cm^{-1} to both medium strong inter- and intra-molecularly bound −O−H stretching modes. We have already noted the two band systems with sub-maxima at 2962, 2922, 2854, 2814, 2756, 2736 and 2597, 2564, 2489, 2474 cm^{-1} in the 3000–2400 cm^{-1} absorption region (see Fig. S1). We assume all these bands to have originated from the strong inter-molecular H-bonding of the −O−H groups in the dimer species. The large red-shifts, 775 and

Table 4

Computed scaled harmonic frequencies (cm^{-1}) for $-$O$-$H and $-$C$=$O modes in monomers and dimers of Chelidonic acid compared with experimental values. The frequencies are calculated at B3LYP/6$-$311++G(d,p) level. All the frequencies (in cm^{-1}) are scaled with the single scaling factor of 0.9688 [51,52].

Experimental		M_1	M_4	D_1	D_2	D_3	D_4	D_5	D_6	Assignments
IR	Raman									
2962	–	–	–	3100	3098	3101	3111	3111	3089	O$-$H stretching (*inter*-bonded)
2922	–	–	–	3009	3007	3010	2982	2982	2998	O$-$H stretching (*inter*-bonded)
3468	–	–	3593	–	–	–	3601	3601	3604	O$-$H stretching (medium strong *inter*-and *intra*-bonded)
3629	–	3615	3620	3614	3623	3624	–	3623	–	O$-$H stretching (free)
3601	–	3614	–	3614	3614	3624	3614	–	–	O$-$H stretching (free)
1648	1646	–	–	1702	1703	1703	1697	1698	1691	C$=$O (carboxyl) stretching (*inter*-bonded)
1723	1736	–	–	1660	1661	1661	1650	1650	1643	C$=$O (carboxyl) stretching (*inter*-bonded)
1830	–	1738	1768	1737	1754	1755	1769	1769	1770	C$=$O (carboxyl) stretching (free)
1452	1444	–	–	1423	1422	1421	1427	1426	1427	O$-$H in-plane bending (*inter*-bonded)
1423	–	–	–	1404	1404	1403	1406	1406	1410	O$-$H in-plane bending (*inter*-bonded)
–	–	–	1162	–	–	–	1158	1158	1158	O$-$H in-plane bending (*intra*-bonded)
1129	1134	1130	1127	1141	1141	1132	1142	1132	–	O$-$H in-plane bending (free)
969	965	–	–	920	921	920	939	939	932	O$-$H out-of-plane bending (*inter*-bonded)
–	–	–	–	851	852	851	849	849	861	O$-$H out-of-plane bending (*inter*-bonded)
603	–	604	564	598	597	565	601	565	–	O$-$H out-of-plane bending (free)

1065 cm^{-1} of the bands at 2854 and 2564 cm^{-1} with respect to the free $-$O$-$H band at 3629 cm^{-1} demonstrates the strong interaction between the $-$O$-$H group of one conformer component and the $-$C$=$O group of another conformer component. For D_1, the bands are calculated at 3100 and 3009 cm^{-1} (Table 4) and are correlated to the observed bands at 2962 and 2922 cm^{-1}. The D_2 and D_3 species show small shifts in these frequencies and are calculated at 3098, 3007 and 3101, 3010 cm^{-1} respectively. For D_4, the frequencies are predicted at 3111 and 2982 cm^{-1}. The two frequencies are comparable with the observed modes at 2962 and 2922 cm^{-1} respectively. For D_5 and D_6 the bands are 3111, 2982 and 3089, 2998 cm^{-1} respectively and are also correlated to the observed bands at 2962 and 2922 cm^{-1}. Clearly, the predicted frequencies at B3LYP/6$-$311++G(d,p) higher level is not much of gain in so far as agreement with the experimental values is concerned. However, we preferred this higher level to a lower level of calculation for reasons of predicting accurate geometries and energies of CA. Further, we tested this premise by performing calculation at BP86/6-31G(d) level as well, yielding satisfactory frequency values for the dimer species (see Table S4). Notwithstanding, the advantage of B3LYP/6$-$311++G(d,p) level will be evident in AIM analysis to be discussed later where computed values of $\rho(\mathbf{r})$ and its Laplacian $\nabla^2\rho(\mathbf{r})$ are more closer to the results reported in the literature [57, 58].

In carboxylic acid dimers, the symmetric and anti-symmetric $-$C$=$O stretching bands show large splitting, as for example, up to 74 cm^{-1} in the formic acid dimer [15, 59]. Of the two possible $-$C$=$O stretching modes, the in-phase carbonyl mode is Raman active and the out-of-phase mode is IR active [15, 59]. In CA, a very strong Raman band appearing at 1646 cm^{-1} and a strong absorption at 1648 cm^{-1} are identified with the H-bonded $-$C$=$O symmetric stretching mode; the anti-symmetric mode is assigned to a strong absorption at 1723 cm^{-1} with a corresponding shoulder Raman band at 1736 cm^{-1} (Table 5). Another strong Raman band at 1750 cm^{-1} is readily assigned to the oxo group $-$C$=$O stretching mode. For the two carboxylic groups in M_1, the free $-$C$=$O stretching modes are predicted at 1738 and 1734 cm^{-1} and for the oxo group it is computed at 1655 cm^{-1} (Table 5). Upon association of the two $-$COOH groups of two different conformer components into an H-bonded dimer, the red-shifts of the carbonyl stretching frequencies are in agreement with the prediction. The symmetric and anti-symmetric carbonyl stretching frequencies for D_4 are predicted at 1650 and 1697 cm^{-1} respectively. The frequencies calculated at 1427, 1406, 1158, 1142 cm^{-1} show contribution from $-$O$-$H in-plane bending mode. The monomeric band for M_1 at 1130 cm^{-1} show blue-shift in the dimer D_4 and the frequency is computed at 1427 cm^{-1}. The corresponding IR band is observed at 1452 cm^{-1} and the Raman band at 1444 cm^{-1}. The *intra*-molecularly bonded $-$O$-$H in-plane bending mode shows a small blue-shift and is predicted at 1162 cm^{-1} for M_4. The out-of-phase $-$O$-$H

bending mode for M_1 is calculated at 604 cm^{-1} and is observed at 603 cm^{-1} as an IR band. In D_4, the two frequencies are calculated at 939 and 849 cm^{-1}; the band at 939 cm^{-1} is observed at 969 cm^{-1} in IR and at 965 cm^{-1} in the Raman spectrum. To conclude, the characteristic blue-shifts in the frequencies of $-$O$-$H deformation vibrations are indicative of the $-$O$-$H group's involvement in the dimerization. As for the modes of other groups, namely, $-$CH, $-$CC and $-$CO below 1400 cm^{-1}, they are all satisfactorily assigned and for the sake of brevity, are summarized in Table 5 (also see Section S7).

3.2. AIM and NCI analysis of H-bonding

The geometrical criterion satisfied by the dimer species derived from DFT calculations alone is not sufficient to characterize the $-$O$-$H$\cdots$O$=$C bonding because computed H-bonded dimer populations for vapor phase do not adequately correspond to possible *inter*-molecular linkages in the solid phase of the sample of CA. The analysis of the topological properties of $\rho(\mathbf{r})$ by Bader's quantum theory of Atoms in Molecule (AIM) is an alternative tool to investigate *inter*-atomic interactions such as H-bonding [37, 38, 41]. The presence of bond critical point (BCP), where the gradient of electron density, $\nabla\rho(\mathbf{r})$, vanishes between two interacting atoms, is a good measure for characterizing the H-bond [37, 38, 39, 40, 41, 42]. Experimentally, the crystal structure determinations by the low-temperature X-ray diffraction (XRD) measurements provide reasonably accurate values of the $\rho(\mathbf{r})$ and $\nabla^2\rho(\mathbf{r})$ [44, 45, 48]. Recently, the *inter*- and *intra*-molecular interactions in crystalline Phthalic acid have been measured from the topology of the electron density distributions obtained from a low temperature (20 K) X-ray diffraction analysis and the values are in good agreement with theoretically-fit values [48]. In the present study, the geometries of the selected CA monomers and dimers showing BCP are presented in Fig. 7a–7d. The AIM analysis has provided BCP for each of the covalently bonded C$-$C, C$-$H, C$-$O, C$=$O and O$-$H groups. The existence of an *intra*-bonding between $-$O$-$H group and pyran ring oxygen in M_4 is evidenced by a BCP between hydrogen and oxygen atom (see Fig. 7b). Each dimer species exhibits two $-$O$-$H$\cdots$O *inter*-molecular H-bonds. The presence of these two bonds is confirmed by two BCPs between the interacting carboxylic groups (see Figs. 7c and 7d). Furthermore, for D_4, a BCP for $-$O$-$H$\cdots$O *intra*-molecular bonding has also been determined. The topological parameters calculated at the BCP values along the O$\cdots$H contacts for the monomer and dimer species of CA are presented in Tables 6a and 6b (see also Table S8a – S8c). On comparing with the values of $\rho(\mathbf{r})$ and $\nabla^2\rho(\mathbf{r})$ computed at the same B3LYP/6$-$311++G(d,p) level for the same H-bonding in 2-pyrrolidine and pyrrole-2-carboxylic acid, we find good agreement with the values computed for CA [57, 58]. However, as for the agreement with the XRD values of Phthalic acid,
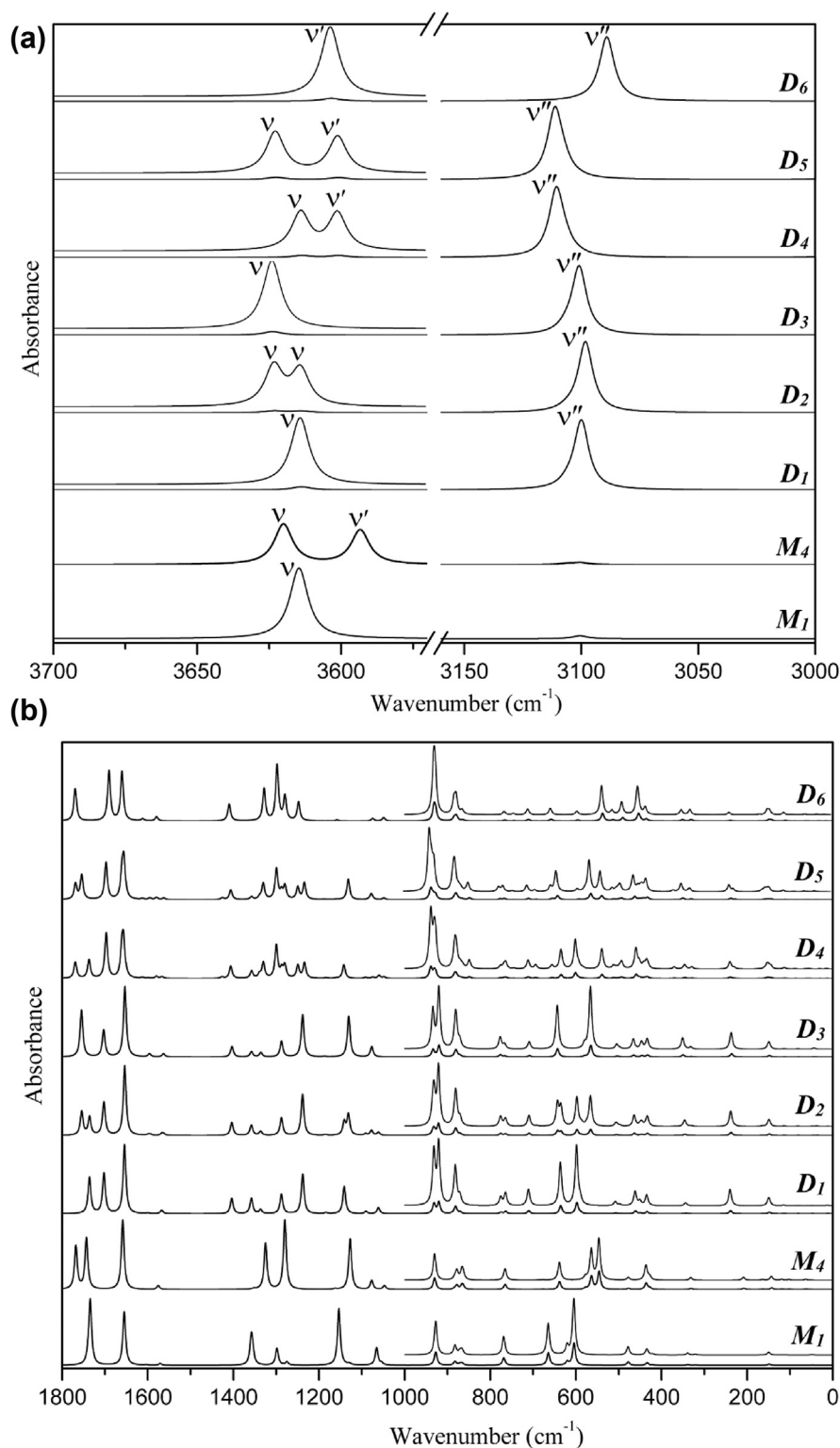
(a)

(b)

Fig. 6. (a) Computed IR spectra of monomers (M_1 and M_4) and dimers (D_1, D_2, D_3, D_4, D_5 and D_6) of Chelidonic acid in the 3700–3000 cm^{-1} region showing dimerization-induced characteristic band shifts and intensity enhancements. Positions of the free −OH stretching bands are marked with ν. The positions of the *intra*- and *inter*-molecular H-bonded −OH stretching bands are marked with ν' and ν'' respectively. In each of the overlaid spectra in the 3700–3500 cm^{-1}, for ease of comparison, the intensities of the free (ν) and H-bonded bands (ν' and ν'') are scaled by a suitable factor. (b) Computed IR spectra of monomers (M_1 and M_4) and dimers (D_1, D_2, D_3, D_4, D_5 and D_6) of Chelidonic acid in the 1800–100 cm^{-1} region showing dimerization-induced characteristic band shifts and intensity enhancements. In each of the overlaid spectra in the 1000–100 cm^{-1}, for ease of comparison, the intensities of the bands are scaled by a suitable factor.

it is not satisfactory with respect to the $\nabla^2 \rho(\mathbf{r})$ values because these are known to vary rapidly at bond curvatures depending on dimer species [39, 40, 41]. It is to be noted that the $\rho(\mathbf{r})$ values, 0.0446–0.0487 a.u. for the *inter*-molecular H-bonds are evidently higher than the values, 0.0217–0.0219 a.u. for the *intra*-molecular bonding (see Tables 6a and 6b).

Noncovalent interactions (NCI) index developed by Johnson *et al* [43] investigates the van der Waals interactions (vdW), steric clashes (SC),

and H-bonds in a molecule based on $\rho(\mathbf{r})$, and their reduced density gradient, $s(\mathbf{r})$, defined as,

$$s(r) = \frac{1}{2(3\pi^2)^{1/3}} \left(\frac{|\nabla \rho(r)|}{[\rho(r)]^{4/3}} \right)$$

An NCI plot of $s(\mathbf{r})$ versus $\rho(\mathbf{r})$ essentially identifies bonding or nonbonding situations by producing the change in $s(\mathbf{r})$ between the interacting units. Further, the value of $\rho(\mathbf{r})$ is a measure of the interaction

Table 5

Experimental IR, Raman and computed scaled harmonic frequencies for monomers (M_1 and M_4) and dimer (D_4) of Chelidonic acid with assignments. sym-symmetric, vs-very strong, s-strong, ms-medium strong, w-weak, vw-very weak, sh-shoulder, oxo-oxo (−C=O) group, carboxyl-carboxyl (−COOH) group. For comparison of the −OH group vibrational modes in the bonded and non-bonded case, monomers M_1 (free), M_4 (*intra*-molecularly bonded) and the dimer D_4 (both *intra*- and *inter*-molecularly bonded) species were chosen. All the frequencies (in cm^{-1}) are scaled with the single scaling factor of 0.9688 [51,52].

| Observed frequencies		Computed frequencies			Assignments [Relative weight (%)]
IR	Raman	Monomer		Dimer	
		M_1	M_4	D_4	
3629 w	–	3615	3620	3614	OH stretch (free) [93]
3601 w	–	3614	–	–	OH stretch (free) [93]
3468 s	–	–	3593	3601	OH stretch (medium strong *inter*- and *intra*-bonded) [96]
2962 ms	–	–	–	3111	OH stretch (*inter*-bonded) [89]
2922 ms	–	–	–	2982	OH stretch (*inter*-bonded) [92]
3127 s	3110 ms	3101	3100	3107, 3101	CH stretch [97]
3055 ms	3055 w	3101	3105	3100, 3100	CH stretch [98]
1830 w	–	1738	1768	1769	C=O (carboxyl) stretch (free) [93]
–	–	1734	1743	1737	C=O (carboxyl) stretch (free) [94]
–	1750 s	1655	1658	1661, 1657	C=O (oxo) stretch (free) [94]
1723 s	1736 sh	–	–	1697	C=O (carboxyl) stretch (bonded) [82]
1648 vs	1646 vs	–	–	1650	C=O (carboxyl) stretch (bonded) [84]
1603 sh	1592 s	1604	1610	1612, 1599	CC stretch (ring) [79], CO (oxo) stretch [6]
1579 vs	1547 s	1571	1575	1580, 1567	CC stretch [78], CH deformation [12]
1452 w	1444 ms	–	–	1427, 1406	COH deformation (bonded) [76], C−COOH stretch [9]
1423 ms	–	1358	1352	1358	CC stretch [60], COH deformation [15], CO (ring) stretch [8]
–	–	1355	1325	1330	CC stretch [72], CO (ring) stretch [13], COH deformation [9]
1370 vw	–	–	–	1339	CC stretch (ring + C−COOH) [53], COH deformation (bonded) [22], CH wag [12]
1315 vw	–	1298	1281	1300	COH deformation [57], CC stretch (ring CC + C−COOH) [22], CH wag [14]
1257 s	1269 ms	1275	1280	1280	CH deformation [65], CC stretch [12], COH deformation [9], CO stretch (ring) [8]
1241 s	–	1181	1179	1183, 1177	CH deformation [83], CC stretch [13]
1204 sh	–	1153	1162	1158	COH deformation [82], C−COOH stretch [11]
1129 s	1134 s	1130	1127	1142	COH deformation [69], CC stretch (ring + C−COOH) [11], CO (ring) stretch [7]
–	1118 s	1065	1077	1091, 1075	CH wag [69], CO stretch (carboxyl) [14], COC scissoring [10]
–	–	1054	1047	1060, 1048	CH wag [53], CO stretch (ring + carboxyl) [24], CC stretch [13]
969 s	965 ms	–	–	939, 849	
921 s	931 w	927	930	931, 928	OH out-of-plane bending (*inter*-bonded) [87] COC (ring)+CCC deformation [81], CH wag [12]
–	906 ms	886	883	890, 888	CH out-of-plane bending [91]
796 ms	796 vw	882	878	883, 883	CH out-of-plane bending [92]
–	790 vw	871	866	880, 878	CCC sym stretch [70], CCH deformation [13], C−COOH stretch [8]
781 w	781 vw	866	863	870, 865	C−COOH stretch [72], ring deformation [16], CO stretch (carboxyl) [8]
743 ms	748 sh	768	765	776, 768	C−COOH torsion [79], ring deformation [14]
–	732 s	757	744	764, 745	C−COOH torsion [79], CH wag [12]
694 s	682 w	687	686	688, 685	CCCO + CCOC torsion [63], CH wag [33]
–	–	664	677	711, 694	COO (carboxyl) bend [69], CC stretch [17], COC (ring) bend [6]
–	–	620	638	656, 634	COO (carboxyl) bend [70], CCC bend [24]
603 w	622 vw	604	564	601	OH out-of-plane bending [94]
–	–	584	547	539	OH out-of-plane bending [93]
535 w	550 sh	581	577	593, 584	C−COOH bend [66], OCC (oxo) in-plane-bending [29]
531 vw	540 ms	506	506	512, 505	CCC bend [64], COC (ring) bend [17], C−CO bend (oxo) [12]
486 wv	487 w	478	477	498, 493	C−COH twist [53], CCOC (ring)+CCCO (oxo) torsion [37]
468 w	467 ms	436	436	451, 450	CCOC torsion [59], CCCO torsion [23], COOH torsion [15]
425	–	434	435	441, 434	OCC (oxo)+CCO (carboxyl) bending [73], CCC (ring) rock [24]
413	387 s	420	427	459, 432	C−COH bending [93]
–	365 ms	338	332	370, 337	CCC + COC (ring) bend [53], ring−COOH torsion [44]
–	261 w	320	331	345, 328	CCO (oxo) bend [50], C−COOH bend [45]
–	201 ms	205	208	239, 229	CCC + CCO (oxo) rock [61], C−COOH rock [29]
–	186 ms	160	163	173, 165	CCCC + CCCO (ring) torsion [82], CCCH torsion [14]
–	150 ms	149	142	149, 144	CCOC (ring)+CCCO (oxo) torsion [90]
–	128 ms	120	118	159, 152	C−COOH in-plane-bending [92]
–	104 vw	109	101	125, 112	CCO (oxo) torsion [51], ring−COOH torsion [45]
–	–	48	63	63, 87	Ring−COOH torsion [98]
–	–	45	52	50, 42	Ring−COOH torsion [94]
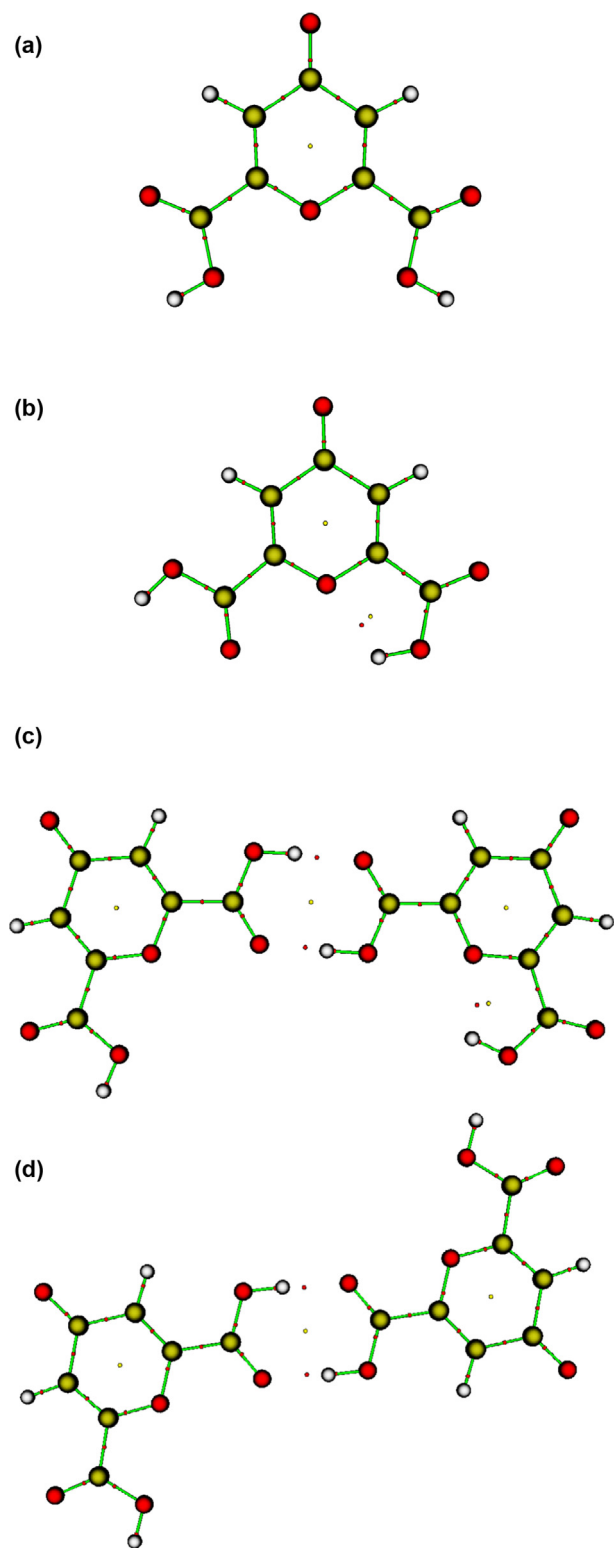
Fig. 7. Molecular structures of monomers and dimers of Chelidonic acid (Fig. 7a – 7d) showing bond critical points (BCP). Topological properties of the electron density at BCP for the O···H contacts computed at B3LYP/6–311++G(d,p) level are presented in Tables 6a and 6b.

strength. The attractive and repulsive interactions are discriminated by multiplying the $\rho(\mathbf{r})$ with the sign of second eigenvalue (λ_2) of the Hessian (a matrix of second-order partial derivatives of $\rho(\mathbf{r})$) [43]. The sign of λ_2 may either be negative or positive depending on the accumulation or depletion of the electron density between the two interacting atoms. The

Table 6a

Topological parameters computed at the O1···H10/O21···H31 bond critical point (BCP) in the monomer and dimer species of Chelidonic acid. All the properties are computed at B3LYP/6–311++G(d,p) level.*Except interaction energy, E_{HB} (kcal/mol), all magnitudes are in a.u. The values of the E_{HB} listed in the above table are computed from potential energy density $V(\mathbf{r})$, by using the expression $E_{HB} = 1/2(V(\mathbf{r}))$ [42].

Species	$\rho(\mathbf{r})$	$\nabla^2\rho(\mathbf{r})$	$V(\mathbf{r})$	*Interaction Energy, E_{HB}	$s*\text{sign}(\lambda_2)\rho(\mathbf{r})$
M_4	0.0219	0.0980	-0.0185	-5.81	-0.0219
D_4	0.0219	0.0975	-0.0185	-5.80	-0.0219
D_5	0.0218	0.0972	-0.0184	-5.77	-0.0218
D_6	0.0217	0.0968	-0.0183	-5.75	-0.0217

former situation corresponds to bonding (vdW and H-bonds) where $\lambda_2 < 0$, while the latter for nonbonding interactions (SC) with $\lambda_2 > 0$. We show in Fig. 8a–8e plots of the $s(\mathbf{r})$ against $\text{sign}(\lambda_2)\rho(\mathbf{r})$ for the monomers and dimers of CA. The plots display the features of the attractive and repulsive NCI in terms of two or more spikes in the low-density and low-gradient regions, while the weak vdW interactions are at near zero density values. Fig. 8b for M_1 shows low-density and low-gradient spikes lying around ±0.01 a.u, being indicative of weak vdW attractions. The spike for SC interactions has appeared at higher positive value. As discussed in the preceding Section 4.1, the M_4 geometry has one intra-molecular H-bond. In Fig. 8c, the low-gradient spike appeared at about $\text{sign}(\lambda_2)\rho(\mathbf{r})$ = -0.0219 a.u is attributed to intra-molecular H-bond in M_4. The $\text{sign}(\lambda_2)\rho(\mathbf{r})$ of -0.0219 a.u for this bond as compared to the vdW interactions (±0.01 a.u) suggests that the intra-molecular H-bonding is relatively strong. The $s(\mathbf{r})$ versus $\text{sign}(\lambda_2)\rho(\mathbf{r})$ plots for the dimer species are shown in Fig. 8d (for D_1 without intra-bonding) and Fig. 8e (for D_4 with intra-bonding) respectively. In Fig. 8d, the low-gradient but high-density spike appeared at $\text{sign}(\lambda_2)\rho(\mathbf{r})$ = -0.0463 a.u, indicating the presence of two strong inter-molecular H-bonds. For D_4, the spikes have appeared at $\text{sign}(\lambda_2)\rho(\mathbf{r})$ = -0.0219 a.u for intra-bond, and -0.0447 and -0.0487 a.u for two inter-bonds. Furthermore, the two inter-molecular H-bonds of D_4 are discriminated as two separate spikes as compared to the one in D_1 due to the differences in the two O···H contact distances (0.033 Å and 0.002 Å respectively, Table S5). Owing to the large $\rho(\mathbf{r})$ values, the H-bonds due to inter-molecular association are stronger than intra-molecular association. This is consistent with the changes in the geometrical parameters and frequencies of the monomer and dimer species discussed in the preceding section 3.1 (see Table 4, Tables S4 and S5). Fig. 8b–8e also show the NCI isosurface plots of the monomer and dimer species calculated at the B3LYP/6–311++G(d,p) level. The blue-green-red (BGR) color scheme is used in which the blue region represents strong attractive interactions (O−H···O bonds) and the green and red regions represent the weak van der Waals (and C−H···O bonds) and strong repulsive steric interactions respectively. The NCI isosurface with a disc shaped volume (red) is characteristic of a strong repulsive steric interaction between the oxygen and carbon atoms of the pyran ring and oxygen of carboxylic groups. The isosurface (green) between the −C−H and −C=O/−C−O groups corresponds to the various weak −C−H···O interactions. The presence of blue-green isosurface between the pyran-ring oxygen and −OH of carboxyl group in the M_4 (Fig. 8c) and D_4 (Fig. 8e) species indicate the presence of the intra-molecular H-bond between the −OH and −CO groups. The blue NCI isosurface between the two carboxylic groups in the D_1 and D_4 species is characteristic of the strong inter-molecular O−H···O bonding. The section S9 (see also Fig. S9a–S9f) presents the correlation of H-bond −OH group stretching frequencies of Chelidonic acid species with the $s*\text{sign}(\lambda_2)\rho(\mathbf{r})$ and interaction energy.

3.3. Natural bond orbital (NBO) analysis

The nature of electronic charge delocalization accompanied by H-bond formation has been investigated by employing NBO analysis [49]. The

Table 6b

Topological parameters computed at the O26···H27 and O16···H17 bond critical points (BCPs) in the dimer species of Chelidonic acid. All the properties are computed at B3LYP/6–311++G(d,p) level.*Except interaction energy, E_{HB} (kcal/mol), all magnitudes are in a.u. The values of the E_{HB} listed in the above table are computed from potential energy density $V(\mathbf{r})$, by using the expression $E_{HB} = 1/2(V(\mathbf{r}))$ [42].

| Species	O···H	$\rho(\mathbf{r})$	$\nabla^2\rho(\mathbf{r})$	$V(\mathbf{r})$	*Interaction Energy, E_{HB}	$s*\text{sign}(\lambda_2)\rho(\mathbf{r})$
D_1	O26···H27	0.0463	0.1366	-0.0435	-13.65	-0.0463
	O16···H17	0.0465	0.1372	-0.0439	-13.76	-0.0465
D_2	O26···H27	0.0464	0.1370	-0.0437	-13.70	-0.0464
	O16···H17	0.0466	0.1372	-0.0439	-13.78	-0.0466
D_3	O26···H27	0.0463	0.1369	-0.0436	-13.69	-0.0463
	O16···H17	0.0463	0.1369	-0.0436	-13.69	-0.0463
D_4	O26···H27	0.0447	0.1350	-0.0416	-13.05	-0.0447
	O16···H17	0.0487	0.1396	-0.0467	-14.64	-0.0487
D_5	O26···H27	0.0446	0.1347	-0.0415	-13.01	-0.0446
	O16···H17	0.0487	0.1398	-0.0467	-14.65	-0.0487
D_6	O26···H27	0.0466	0.1374	-0.0440	-13.81	-0.0466
	O16···H17	0.0466	0.1374	-0.0440	-13.81	-0.0466

(a)

(b)

(c)

(d)
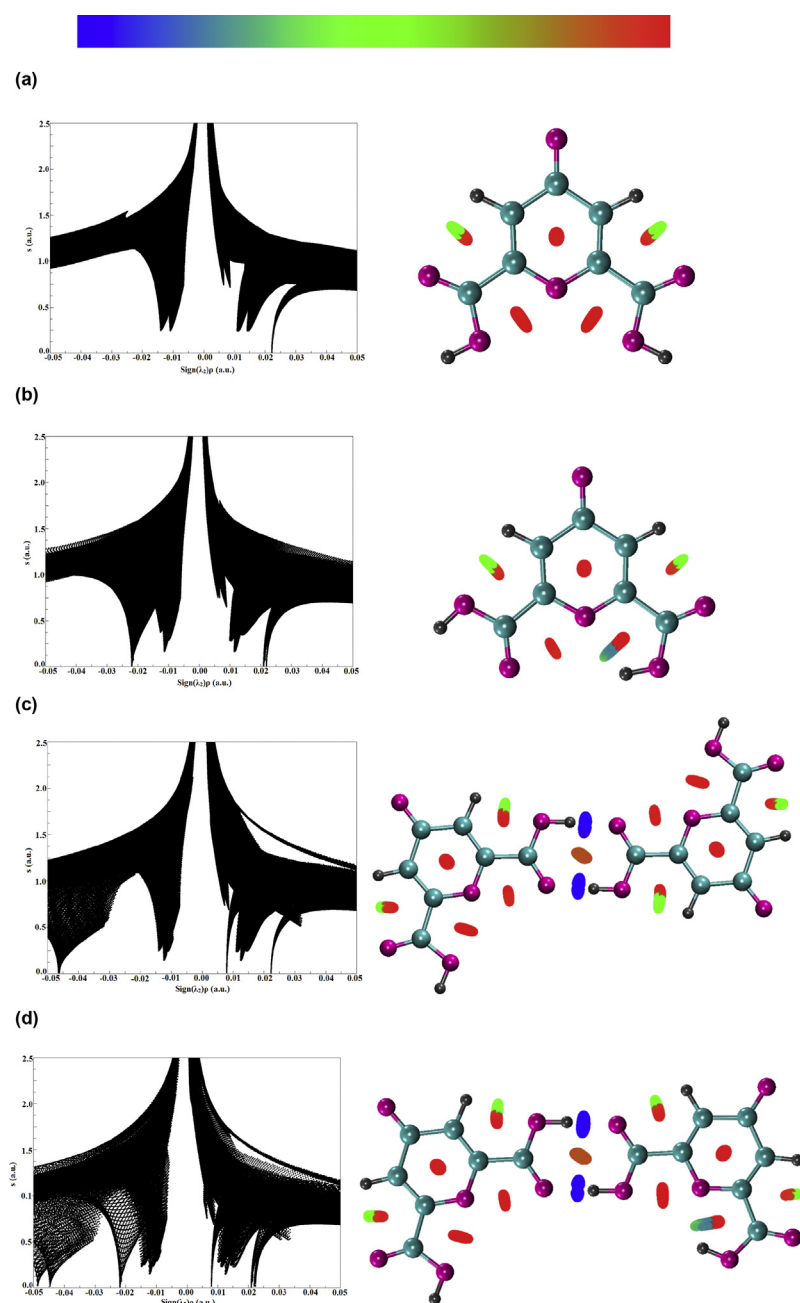
Fig. 8. Plots of the reduced density gradient, *s, versus* the electron density $\rho(\mathbf{r})$, multiplied by the sign of second eigenvalue (λ_2) of the electron-density Hessian matrix, $\text{sign}(\lambda_2)\rho(\mathbf{r})$ (left) and the corresponding isosurfaces with isovalue = 0.5 a.u (right) for Chelidonic acid structures. Isosurfaces are colored according to a BGR color scheme (Fig. 8a). Blue indicates strong attraction regime (*intra-/inter-* H-bonding), green indicates weak interaction regime (such as −C−H···O and van der Waals attraction), and red indicates strong repulsion regime (steric clashes). The 2D NCI plots are shown for M_1 (Fig. 8b) and M_4 (Fig. 8c) monomers and for D_1 (Fig. 8d) and D_4 (Fig. 8e) dimer structures. In each of the plots, the low-gradient spikes at about $\text{sign}(\lambda_2)\rho(\mathbf{r}) = \pm 0.01$ a.u represents the weak van der Waals interactions. The spikes at about $\text{sign}(\lambda_2)\rho(\mathbf{r}) = -0.0219$ a.u and $\text{sign}(\lambda_2)\rho(\mathbf{r}) = -0.0487$ a.u represents the *intra-* and *inter-* molecular H-bonds respectively.

Table 7a

Natural charges (NC) of atoms participating in H-bondings as computed by natural bond orbital (NBO) method. The NC are calculated at B3LYP/6–311++G(d,p) level.

Atom	M_1	M_4	D_1	D_2	D_3	D_4	D_5	D_6
O16	-0.6559	-0.6705	-0.6266	-0.6271	-0.6233	-0.6277	-0.6237	-0.6431
H17	0.4906	0.4956	0.5196	0.5173	0.52010	0.5171	0.5173	0.5173
O18	–	–	-0.6698	-0.6696	-0.6708	-0.6610	-0.6624	-0.6593
O26	–	–	-0.6269	-0.6229	-0.6282	-0.6417	-0.6409	-0.6404
H27	–	–	0.5198	0.5201	0.5177	0.5194	0.5170	0.5172
O15	-0.5676	-0.5563	-0.6698	-0.6687	-0.6684	-0.6679	-0.6674	-0.6591
O1/O21	-0.4496	-0.4938	-0.4465	-0.4466	-0.4413	-0.4969	-0.4979	-0.4990
H10/H31	0.4906	0.4964	0.4912	0.4911	0.4937	0.4943	0.4946	0.4938
O9/O30	-0.6559	-0.6530	-0.5668	-0.6538	-0.6777	-0.6531	-0.6526	-0.6523

Table 7b

Strength of the H-bonded structures (dimers) of Chelidonic acid as computed by natural bond orbital (NBO) analysis at B3LYP/6–311++G(d,p) level. All the numbers are in kcal/mol. n-refers to oxygen atom lone-pair orbital, σ^*-refers to −OH anti-bonding orbital.

Delocalization	D_1	D_2	D_3	D_4	D_5	D_6
$n(O16) \rightarrow \sigma^*(O18-H17)$	28.08	28.71	27.95	30.89	30.93	28.78
$n(O26) \rightarrow \sigma^*(O15-H27)$	27.79	27.88	28.37	26.05	26.54	28.69
$n(O1) \rightarrow \sigma^*(O9-H10)$	–	–	–	–	–	1.62
$n(O21) \rightarrow \sigma^*(O30-H31)$	–	–	–	1.50	1.70	1.59

charge delocalization, in many cases, influences the conformational behavior, H-bond strengths and IR modes. The natural charges (NC) of the atoms and stabilization energy defined as the strength of the charge transfer between oxygen lone pair orbitals and −OH anti-bonding orbital have been computed to identify and confirm the single/double H-bond structures of CA. In all the D_1, D_2, D_3, D_4, D_5 and D_6 species, the lone pair orbitals of the carbonyl oxygen and anti-bonding orbital of the hydroxyl group have been identified as the donor and acceptor sites. The natural charges for some selected atoms collected from natural population analysis are presented in Table 7a. As can be seen from Table 7a, on account of the association between the two −COOH groups exchanging natural charges, their simultaneous H-bond donor-acceptor behavior is confirmed. As compared to the monomers, in D_4, the atoms O16 and O26 become positive as they H-bond with O18−H17 and O15−H27 respectively. On the other hand, O18 and O15 in the hydroxyl groups gain some charges through inter-molecular O−H···O dimerization. The bridging atoms, H17 and H27, become slightly more positive. The stabilization energies obtained from the NBO analysis are presented in Table 7b. All the dimers exhibit two inter-molecular donor-acceptor interactions or hyperconjugations defined as $n(O16) \rightarrow \sigma^*(O18-H17)$ and $n(O26) \rightarrow \sigma^*(O15-H27)$. The D_1 and D_2 are characterized by the net energy of 55.87 and 56.59 kcal/mol and D_3 and D_4 species are stabilized by 56.32 and 56.94 kcal/mol respectively. The analysis of Table 7b shows that the two inter-molecular H-bonds in the dimer D_5 and D_6 are characterized by the net stabilization energy of 57.47 kcal/mol. In addition to two inter-molecular interactions, D_4 and D_5 exhibit $n(O21) \rightarrow \sigma^*(O30-H31)$ intra-molecular interaction with the stabilization energies of 1.50 and 1.70 kcal/mol. The two intra-molecular bonding in D_6 (see Fig. 4) are confirmed by $n(O1) \rightarrow \sigma^*(O9-H10)$ and $n(O21) \rightarrow \sigma^*(O30-H31)$ hyperconjugations with stabilization energy at 1.62 and 1.59 kcal/mol respectively. The estimation of the natural charges and stabilization energy of the H-bonds by NBO analysis for the dimer species of the CA confirms the presence of intra- and inter-molecular H-bonding interactions with the latter H-bonding stronger than the former. Consequently, the hydroxyl groups participating in intra-bonding show less red-shift compared to the inter-bonding, and we correlate this to two separate observed IR bands at 3468 and 2962 cm^{-1} respectively (see Fig. 2 and Fig. S1). The electron donor (−C=O) and acceptor (−OH) sites participated in the hyperconjugation interactions show weakening of bond strengths due to the charge transfer to −OH anti-bonding orbital. Therefore, the increase in the bond lengths and red-shift in the stretching vibrations of the carbonyl and hydroxyl groups are the consequences of the electronic charge delocalization.

4. Conclusions

The −O−H···O H-bond mediated composite vibrational structure observed in the IR and Raman spectra (4000–100 cm^{-1}) of Chelidonic acid has been characterized by the structures, interaction energies and harmonic frequencies for the ten monomer and six dimer species computed at B3LYP/6–311++G(d,p) and BP86/6-31G(d) levels. The AIM analysis has provided additional support to the H-bond characterization in terms of BCP values for both intra- and inter-molecular −O−H···O H-bonding. The existence of the both type of H-bonding has been demonstrated by BCPs for each of the O···H contacts. The electron density plots have provided insights into the nature of the H-bonds. The weak van der Waals and H-bonding interactions exhibited low-gradient spikes at BCPs having different magnitudes of electron densities. The calculation of the natural charges and stabilization energy of the H-bonds for the dimer species by NBO analysis further points to the presence of the stronger inter-molecular H-bonding interactions than the intra-H-bonding. It has been noted that while the geometries and interaction energies are accurately predicted at B3LYP/6–311++G(d,p), the BP86/6-31G(d) level is shown to produce slightly more accurate frequencies. However, the benefits of the B3LYP/6–311++G(d,p) level outweighs when it produced better results for the AIM and NCI calculations. The proposed dimer model is to be treated as a basic unit in oligomers that may make up Chelidonic acid in its solid phase.

References

[1] P. Rodziewicz, N.L. Doltsinis, Formic acid dimerization: evidence for species diversity from first principles simulations, J. Phys. Chem. A 113 (2009) 6266–6274.

[2] R.M. Balabin, Polar (acyclic) isomer of formic acid dimer: gas-phase Raman spectroscopy study and thermodynamic parameters, J. Phys. Chem. A 113 (2009) 4910–4918.

[3] A. Olbert-Majkut, J. Ahokas, J. Lundell, M. Pettersson, Raman spectroscopy of formic acid and its dimers isolated in low temperature argon matrices, Chem. Phys. Lett. 468 (2009) 176–183.

[4] K. Marushkevich, L. Khriachtchev, J. Lundell, A. Domanskaya, M. Räsänen, Matrix isolation and ab initio study of Trans−Trans and Trans−Cis dimers of formic acid, J. Phys. Chem. A 114 (2010) 3495–3502.

[5] K. Marushkevich, M. Siltanen, M. Räsänen, L. Halonen, L. Khriachtchev, Identification of New dimers of formic acid: the use of a continuous-wave optical parametric oscillator in matrix isolation experiments, J. Phys. Chem. Lett. 2 (2011) 695–699.

[6] K. Marushkevich, L. Khriachtchev, M. Räsänen, M. Melavuori, J. Lundell, Dimers of the higher-energy conformer of formic acid: experimental observation, J. Phys. Chem. A 116 (2012) 2101–2108.

[7] N.R. Brinkmann, G.S. Tschumper, G. Yan, H.F. Schaefer, An alternative mechanism for the dimerization of formic acid, J. Phys. Chem. A 107 (2003) 10208–10216.

[8] M. Zahedi-Tabrizi, R. Farahati, Calculation of intramolecular hydrogen bonding strength and natural bond orbital (NBO) analysis of naphthazarin with chlorine substitution, Comput. Theor. Chem. 977 (2011) 195–200.

[9] M. Karabacak, M. Cinar, M. Kurt, P. Chinna babu, N. Sundaraganesan, Experimental and theoretical FTIR and FT-Raman spectroscopic analysis of 1-pyrenecarboxylic acid, Spectrochim. Acta 114 (2013) 509–519.

[10] E. Sanchez-Garcia, L.A. Montero, W. Sander, Computational study of noncovalent complexes between formamide and formic acid, J. Phys. Chem. A 110 (2006) 12613–12622.

[11] M. Ortlieb, M. Havenith, Proton transfer in (HCOOH)$_2$: an IR high-resolution spectroscopic study of the antisymmetric C−O stretch, J. Phys. Chem. A 111 (2007) 7355–7363.

[12] R. Kalescky, E. Kraka, D. Cremer, Accurate determination of the binding energy of the formic acid dimer: the importance of geometry relaxation, J. Chem. Phys. 140 (2014) 084315−1–084315−8.

[13] K.G. Goroya, Y. Zhu, P. Sun, C. Duan, High resolution jet-cooled infrared absorption spectra of the formic acid dimer: a reinvestigation of the C−O stretch region, J. Chem. Phys. 140 (2014) 164311−1–164311−6.

[14] W. Qian, S. Krimm, Origin of the C=O stretch mode splitting in the formic acid dimer, J. Phys. Chem. 100 (1996) 14602–14608.

[15] J. Dybal, T.C. Cheam, S. Krimm, C=O stretch mode splitting in the formic acid dimer: electrostatic models of the intermonomer interaction, J. Mol. Struct. 159 (1987) 183–194.

[16] G.N.R. Tripathi, S.J. Sheng, Solid-state vibrational spectra and structures of terephthalic acid and the terephthalate ion, J. Mol. Struct. 57 (1979) 21–34.

[17] L. Colombo, V. Volovšek, M. Lepostollec, Vibrational analysis and normal coordinate calculations of the o-phthalic acid molecule, J. Raman Spectrosc. 15 (4) (1984) 252–256.

[18] C.A. Téllez S, E. Hollauer, M.A. Mondragon, V.M. Castaño, Fourier transform infrared and Raman spectra, vibrational assignment and ab initio calculations of terephthalic acid and related compounds, Spectrochim. Acta 57 (2001) 993–1007.

[19] F. Bardak, C. Karaca, S. Bilgili, A. Atac, T. Mavis, A.M. Asiri, M. Karabacak, E. Kose, Conformational, electronic, and spectroscopic characterization of isophthalic acid (monomer and dimer structures) experimentally and by DFT, Spectrochim. Acta 165 (2016) 33–46.

[20] M. Lackinger, S. Griessl, T. Markert, F. Jamitzky, W.M. Heckl, Self-assembly of Benzene−Dicarboxylic acid isomers at the liquid solid interface: steric aspects of hydrogen bonding, J. Phys. Chem. B 108 (2004) 13652–13655.

[21] H.T. Flakus, B. Hachuła, J.T. Hołaj-Krzak, F.A. Al-Agel, N. Rekik, Long-distance" H/D isotopic self-organization phenomena in scope of the infrared spectra of hydrogen-bonded terephthalic and phthalic acid crystals, Spectrochim. Acta 173 (2017) 65–74.

[22] H.H. Pham, C.D. Taylor, N.J. Henson, First-principles prediction of the effects of temperature and solvent selection on the dimerization of benzoic acid, J. Phys. Chem. B 117 (2013) 868–876.

[23] N. Martsinovich, A. Troisi, Modeling the self-assembly of benzenedicarboxylic acids using Monte Carlo and molecular dynamics simulations, J. Phys. Chem. C 114 (2010) 4376–4388.

[24] R. Alcala, S. Martinez-Carrera, The crystal structure of isophthalic acid, Acta Crystallogr. B28 (1972) 1671–1677.

[25] J.L. Derissen, The crystal structure of isophthalic acid, Acta Crystallogr. B30 (1974) 2764–2765.

[26] J. Mi, L. Chen, M. He, 5-Fluoro-isophthalic acid, Acta Crystallogr. E67 (2011) o590.

[27] D. Kim, S. Kim, M. Kim, Y. Jeon, J. Um, S. Hong, The therapeutic effect of chelidonic acid on ulcerative colitis, Biol. Pharm. Bull. 35 (5) (2012) 666–671.

[28] T.G. Porter, D.L. Martin, Chelidonic acid and other conformationally restricted substrate analogues as inhibitors of rat brain glutamate decarboxylase, Biochem. Pharmacol. 34 (1985) 4145–4150.

[29] C.E. Carraher Jr., M.R. Roner, M. Ayoub, N. Pham, A. Moric-Johnson, Synthesis and preliminary cancer activity of chelidonic acid containing polyesters containing the triphenylarsenic, triphenylantimony, and triphenylbismuth moiety, Int. J. Polym. Mater. 64 (2015) 311–319.

[30] M.J. Frisch, G.W. Trucks, H.B. Schlegel, G.E. Scuseria, M.A. Robb, J.R. Cheeseman, G. Scalmani, V. Barone, B. Mennucci, G.A. Petersson, H. Nakatsuji, M. Caricato, X. Li, H.P. Hratchian, A.F. Izmaylov, J. Bloino, G. Zheng, J.L. Sonnenberg, M. Hada, M. Ehara, K. Toyota, R. Fukuda, J. Hasegawa, M. Ishida, T. Nakajima, Y. Honda, O. Kitao, H. Nakai, T. Vreven, J.A. Montgomery Jr., J.E. Peralta, F. Ogliaro, M. Bearpark, J.J. Heyd, E. Brothers, K.N. Kudin, V.N. Staroverov, R. Kobayashi, J. Normand, K. Raghavachari, A. Rendell, J.C. Burant, S.S. Iyengar, J. Tomasi, M. Cossi, N. Rega, J.M. Millam, M. Klene, J.E. Knox, J.B. Cross, V. Bakken, C. Adamo, J. Jaramillo, R. Gomperts, R.E. Stratmann, O. Yazyev, A.J. Austin, R. Cammi, C. Pomelli, J.W. Ochterski, R.L. Martin, K. Morokuma, V.G. Zakrzewski, G.A. Voth, P. Salvador, J.J. Dannenberg, S. Dapprich, A.D. Daniels, Ö. Farkas, J.B. Foresman, J.V. Ortiz, J. Cioslowski, D.J. Fox, Gaussian 09, Revision D.01, Gaussian, Inc., Wallingford CT, 2013.

[31] R. Dennington, T. Keith, J. Millam, GaussView 5.0, Semichem Inc. Shawnee Mission, KS, 2009.

[32] T. Lu, F. Chen, Multiwfn: a multifunctional wavefunction analyzer, J. Comput. Chem. 33 (2012) 580–592.

[33] T. Lu, F. Chen, Quantitative analysis of molecular surface based on improved Marching Tetrahedra algorithm, J. Mol. Graph. Model. 38 (2012) 314–323.

[34] W. Humphrey, A. Dalke, K. Schulten, VMD: visual molecular dynamics, J. Mol. Graph. 14 (1996) 33–38.

[35] ChemCraft 1.8, https://www.chemcraftprog.com.

[36] S.F. Boys, F. Bernardi, The calculation of small molecular interactions by the differences of separate total energies. Some procedures with reduced errors, Mol. Phys. 19 (1970) 553–566.

[37] R.F.W. Bader, A quantum theory of molecular structure and its applications, Chem. Rev. 91 (1991) 893–928.

[38] R.F.W. Bader, Atoms in Molecules: A Quantum Theory, Clarendon Press, Oxford, U.K., 1990.

[39] U. Koch, P.L.A. Popelier, Characterization of C-H-O hydrogen bonds on the basis of the charge density, J. Phys. Chem. 99 (1995) 9747–9754.

[40] P.L.A. Popelier, Characterization of a dihydrogen bond on the basis of the electron density, J. Phys. Chem. A 102 (1998) 1873–1878.

[41] P.L. Popelier, Atoms in Molecules: an Introduction, Prentice Hall, Englewood Cliffs, NJ, 2000.

[42] E. Espinosa, E. Molins, C. Lecomte, Hydrogen bond strengths revealed by topological analyses of experimentally observed electron densities, Chem. Phys. Lett. 285 (1998) 170–173.

[43] E.R. Johnson, S. Keinan, P. Mori-Sanchez, J. Contreras-Garcia, A.J. Cohen, W. yang, Revealing noncovalent interactions, J. Am. Chem. Soc. 132 (2010) 6498–6506.

[44] C. Gatti, P. Macchi, Modern Charge Density Analysis, Springer, New York, 2012.

[45] P. Coppens, Charge-density analysis at the turn of the century, Acta Crystallogr. A54 (1998) 779–788.

[46] D. Chopra, Advances in understanding of chemical bonding: inputs from experimental and theoretical charge density analysis, J. Phys. Chem. A 116 (2012) 9791–9801.

[47] G. Saleh, C. Gatti, L.L. Presti, Energetics of non-covalent interactions from electron and energy density distributions, Comput. Theor. Chem. 1053 (2015) 53–59.

[48] V.V. Zhurov, A. Alan Pinkerton, Quantifying the inter- and intramolecular interactions in crystalline phthalic acid, Cryst. Growth Des. 14 (2014) 5685–5691.

[49] A.E. Reed, L.A. Curtiss, F. Weinhold, Intermolecular interactions from a natural bond orbital, donor-acceptor viewpoint, Chem. Rev. 88 (1988) 899–926.

[50] M. St, C. Flett, The characteristic infra-red frequencies of the carboxylic acid group, J. Chem. Soc. 0 (1951) 962–967.

[51] L.M.N.B.F. Santos, M.A.A. Rocha, Gaseous phase heat capacity of benzoic acid, J. Chem. Eng. Data 55 (2010) 2799–2808.

[52] J.P. Merrick, D. Moran, L. Radom, An evaluation of harmonic vibrational frequency scale factors, J. Phys. Chem. A 111 (2007) 11683–11700.

[53] G.R. Desiraju, T. Steiner, The Weak Hydrogen Bond: in Structural Chemistry and Biology, Oxford Univ. Press, Inc., New York, 2001.

[54] G. Allen, G.J. Watkinson, K.H. Webb, An infra-red study of the association of benzoic acid in the vapour phase, and in dilute solution in non-polar solvents, Spectrochim. Acta 22 (1966) 807–814.

[55] G. Allen, E.F. Caldin, Determination of the thermodynamic data for the dimerization of some carboxylic acids in benzene by a boiling-point method, Trans. Faraday Soc. 49 (1953) 895–905.

[56] S. Lovell, P. Subramony, B. Kahr, Poppy acid: synthesis and crystal chemistry, J. Am. Chem. Soc. 121 (1999) 7020–7025.

[57] A.E. Shchavlev, A.N. Pankratov, V.B. Borodulin, O.A. Chaplygina, DFT study of the monomers and dimers of 2-pyrrolidone: equilibrium structures, vibrational, orbital, topological, and NBO analysis of hydrogen-bonded interactions, J. Phys. Chem. A 109 (2005) 10982–10996.

[58] S.J. Grabowski, A.T. Dubis, D. Martynowski, M. Glowka, M. Palusiak, J. Leszczynski, Crystal and molecular structure of pyrrole-2-carboxylic acid; π-electron delocalization of its Dimers−DFT and MP2 calculations, J. Phys. Chem. A 108 (2004) 5815–5822.

[59] J.E. Bertie, K.H. Michaelian, H.H. Eysel, D. Hager, The Raman-active O–H and O–D stretching vibrations and Raman spectra of gaseous formic acid-d$_1$ and -OD, J. Chem. Phys. 85 (1986) 4779–4789.